

Molecularly imprinted polymers electrochemical sensing: the effect of inhomogeneous binding sites on the measurements. Comparison between imprinted polyaniline *versus* nanoMIP-doped polyaniline electrodes for the EIS detection of 17 β -estradiol.

Alice Marinangeli^{1‡}, Iva Chianella^{2‡}, Eros Radicchi¹, Devid Maniglio³, Alessandra Maria Bossi^{1*}

AUTHOR ADDRESS

¹ University of Verona, Department of Biotechnology, Strada Le Grazie 15, 37134, Verona, Italy;

² Cranfield University, Surface Engineering and Precision Centre, School of Aerospace, Transport and Manufacturing, Bedford, MK43 0AL, United Kingdom;

³ University of Trento, Department of Industrial Engineering, Via Sommarive 9, 38123, Povo, Trento, Italy.

KEYWORDS: *Molecularly imprinted polymers, molecularly imprinted nanoparticles, polyaniline, homogeneous binding sites, heterogeneous binding sites, electrochemical impedance spectroscopy, 17 β -estradiol, water pollution.*

ABSTRACT: Molecularly imprinted polymers (MIPs) are synthetic receptors made by a template-assisted synthesis. MIPs might be ideal receptors for sensing devices, given the possibility to custom-design selectivity and affinity towards a targeted analyte and for their robustness and ability to withstand harsh conditions. However, the synthesis of MIP is an inherently random process, which produces a statistical distribution of binding sites, characterized by a variety of affinities. This is verified both for bulk MIP materials and for MIP's thin layers. In the present work, we aimed at assessing the effects of inhomogeneous *versus* homogeneous imprinted binding sites on electrochemical sensing measurements, and the possible implications on the sensor's performance. In the example of an Electrochemical Impedance Spectroscopy (EIS) sensor for the 17 β -estradiol (E2) hormone, the scenario of inhomogeneous binding sites was studied modifying electrodes with an E2-MIP polyaniline (PANI) thin layer, called: "Imprinted PANI layer". In contrast, the condition of discrete and uniform binding sites was epitomized by electrodes modified with a thin PANI layer purposely doped with E2-MIP nanoparticles (nanoMIPs), that were referred to as "nanoMIP-doped PANI". The behaviours of the two EIS-sensors were compared. Interestingly, the sensitivity of the nanoMIP-doped PANI was almost twice with respect to that of the imprinted PANI layer, strongly suggesting that the homogeneity of the binding sites has a fundamental role in sensor's development. The nanoMIP-doped PANI sensor, which showed a response for E2 in the range 36.7 pM-36.7 nM and had a LOD of 2.86 pg/mL, was used to determine E2 in wastewaters.

Molecularly imprinted polymers (MIPs) are synthetic polymers engineered to have selective binding sites for specific target analytes.^{1,2} MIPs are prepared through a template-assisted polymerization, in which the target analyte acts as a template. Briefly, solvated functional monomers form a complex with the template, which is next fixed through polymerization. At the completion of the

synthesis, the removal of the template frees molecular cavities that are complementary in size, shape, and functional group's stereo-arrangements to the target analyte. As a result, MIPs display the ability to specifically and selectively re-bind the targeted analyte, qualifying as ideal receptors for sensing applications.

A challenge in molecular imprinting is posed by the heterogeneity of the binding sites formed through the imprinting process. Not all the sites stamped in the MIP material possess identical affinity and specificity for the target analyte, leading to variability in binding efficiency and selectivity.³ Such heterogeneity is due to variations in the polymerization process,⁴ such as the template orientation in the nascent material, an excess of functional groups in the polymer, the distribution of functional groups in the polymeric network, and ultimately the accessibility of the formed binding sites (Figure 1A), with possible detrimental effects on the performance and the reproducibility of the MIP-based sensing measurements.

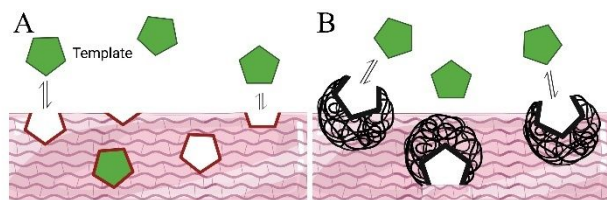


Figure 1. Scheme depicting the heterogeneity of binding sites formed by means of the molecularly imprinting process, in the case of electropolymerization of PANI (A); homogeneous binding sites obtained by doping with nanoMIPs PANI (B).

The issue of heterogeneous binding sites is particularly severe for MIPs prepared in bulk formats, where no control could be attained over the synthesis of the macro-polymer, nor, later, over the accessibility of the imprinted sites.³ Electropolymerization of MIP's thin films, starting from semiconducting monomers, has gained momentum, offering superior control over the thickness of the nascent MIP layers, being it easily attained by varying the number of electropolymerization cycles, with the ultimate effect of gaining higher control over the imprinted sites. As a result, MIP thin films, prepared by electropolymerization, are widely employed in sensing.⁵⁻¹⁰ Despite favourable binding kinetics and reproducibility of the synthetic processes, the expectations over the homogeneity of the binding sites produced by electropolymerization of MIP thin films seem somehow contradicted by binding data reported in the literature, which are often best-fitted with isotherm equations that contain a heterogeneity parameter.^{11,12}

Several authors have critically discussed the equation-models to fit experimental data of an analyte that binds to the MIP.^{4,13,14} Briefly, the Langmuir equation is specific to describe binding processes where an analyte binds to a homogeneous surface with a finite number of identical binding sites. Langmuir model is expressed by the formula: $q_e = q_m K_L [L] / (1 + K_L [L])$, where q_e is the amount of adsorbate per unit mass of adsorbent; q_m is the maximum amount of adsorbate per unit mass of adsorbent; $[L]$ is the concentration of adsorbate; K_L is the Langmuir constant.

Instead, equations meant to describe heterogeneous binding sites are the Freundlich or the Sips models. The Freundlich isotherm is used for describing adsorption on heterogeneous surfaces and is expressed by the equation: $q_e = K_F [L]^{1/n}$, where q_e is the amount of adsorbate per unit mass of adsorbent; $[L]$ is the concentration of adsorbate; K_F is the Freundlich constant; $1/n$ is a heterogeneity factor.

Freundlich model assumes a non-uniform distribution of binding sites and does not assume a fixed number of identical binding sites. Overall, Freundlich isotherm gives a general description of adsorption capacity across a range of concentrations. As an alternative, the Langmuir-Freundlich isotherm, also called Sips isotherm, can be used. Sips equation has the following expression: $q_e = K_S [L]^n (1 + K_S [L]^n)^{-1/n}$, where q_e is the amount of adsorbate per unit mass of adsorbent; $[L]$ is the concentration of adsorbate; K_S is the Sips constant and n is the heterogeneity factor, indicating the degree of non-linearity between solution concentration and adsorption. Sips is a model that combines features of both the Langmuir and Freundlich isotherms, making it suitable for heterogeneous surfaces with a finite number of binding sites. Frequently, the binding of an analyte to its MIP is fitted with the Hill equation, whose expression is: $\theta = [L]^n / (K_d + [L]^n)$, where θ is the fraction of binding sites occupied; $[L]$ is the ligand concentration; K_d is the dissociation constant and n is the Hill coefficient, which is a coefficient intended to indicate cooperativity ($n > 1$ indicates positive cooperativity; $n = 1$ indicates non-cooperative (independent) binding; $n < 1$ indicates negative cooperativity). The Hill equation model is meant to describe cooperative binding rather than the heterogeneity of binding sites. However, it can provide insights into apparent heterogeneity, through its description of cooperative effects. In fact, Hill model can reflect apparent heterogeneity if $n \neq 1$, with the *caveat* that it does not explicitly account for different binding affinities among various sites on the surface.

Very often, the most accurate descriptor of the interaction between an analyte and the MIP-sensor's surface is a model equation that include heterogeneity, such as Hill, Freundlich, Sips equation models, with $n \neq 1$, suggesting the presence of non-uniform binding sites.^{11,15}

The present work is intended to assess which effects do inhomogeneous *versus* homogeneous imprinted binding sites have on the electrochemical sensing measurements and whether heterogeneity has possible implications on the efficiency of the sensor's performance.

To simulate the different scenarios, we compared the sensing measurements from electrodes modified with a polyaniline (PANI) MIP thin layer, called "imprinted PANI layer" and epitomizing the inhomogeneous imprinted binding sites condition (Figure 1A), with electrodes prepared with an electrochemically deposited PANI thin layer purposely doped with MIP nanoparticles (nanoMIPs), that acted as discrete and uniform three-dimensional selective binding sites and were called "nanoMIP-doped PANI" (Figure 1B). The model of uniform binding sites, as shown in Figure 1B, assumes a simplified two-state condition system, in which the binding sites are either accessible, or non-accessible to the analyte, depending on the orientation of the nanoMIPs dispersed in the PANI layer.

The target analyte selected for the comparison was 17β -estradiol (E2), an estrogen hormone, vital for human biology and physiology, playing crucial roles in regulating reproduction, cardiovascular health, gastrointestinal processes, bone strength, cognitive behaviour, and

pregnancy. Released in the environment, for its industrial, agricultural and feed production uses, E2 has anabolic effects disruptive both for aquatic ecosystems and humans.¹⁶ In fact, E2 is classified as an endocrine-disrupting chemical, interfering with normal endocrine function. Consequently, it is crucial to ensure that E2 levels in the environment remain below accepted No-Observed Effect Levels (NOELs).^{17,18}

Electrochemical sensors to determine E2 have long been developed, in view of offering fast and accurate information in a cost-effective manner.¹⁹ Several E2 selective MIPs have been reported as receptor elements with the aim of improving the selectivity of the sensors.²⁰ Among these, an E2 MIP sensor was prepared from a versatile monomer N-phenylethylene diamine methacrylamide (NPEDMA),²¹ by the electropolymerization of the aniline moiety of NPEDMA onto the surface of the electrode, followed by an orthogonally polymerized MIP layer. As a result, the MIP sensor displayed a limit of detection (LOD) of 6.86×10^{-7} M with a linearity range between 1×10^{-7} M and 8×10^{-7} M. Higher sensitivities and lower LODs were reported for electrically conducting materials, such as carbon nanotubes, graphene, and noble metal nanoparticles, deposited at the interface between the electrode and the MIP.⁷ Yuan et al. deposited platinum nanoparticles (PtNPs) onto the electrode, so to increase the surface area, hence the conductivity, followed by 6-mercaptopuric acid (MNA) self-assembling at the PtNPs/GCE surface in the presence of the template E2 and electropolymerization.²² Differential pulse voltammetry (DPV) detected E2 in the linear range 30 nM–50 μ M with a LOD of 16 nM. Additionally, a sandwich-type molecular imprinting electrochemical sensor (MIES) for the determination of E2 in makeups was prepared onto doubly layered reduced graphene oxide (rGO) combined with PtNPs and a MIP film made by the electropolymerization of MNA in the presence of E2.²³ DPV measurements showed a LOD of 2 nM and two linear regions, namely 4–60 nM and 60 nM–50 μ M, supporting the heterogeneity of the MIP binding sites.

Electrochemical Impedance Spectroscopy (EIS)^{24,25} with gold nanoparticles (AuNPs), instead of PtNPs,²⁶ and a p-aminothiophenol (ATP) electropolymerized E2-MIP, permitted the determination of E2 in milk with a LOD of 1.28 fg/mL and a linear detection range from 1.0 fg/mL to 100 pg/mL. Instead, E2 detection in river waters was reported by Florea et al.²⁷ with linear sweep voltammetry, LOD of 1.09 fM (0.297 fg/mL) and a linear detection range from 3.6 fM to 3.6 nM (corresponding to 0.981 fg/mL to 0.981 ng/mL).

In the present work, we attempted to study the specific contribution given by the templated binding sites to the sensor's signal. For this, we compared screen-printed gold electrodes (gold SPE) modified with an "imprinted PANI layer", that would presumably bear non-uniform binding sites, to gold SPE modified with a nanoMIP-doped PANI, to simulate discrete and uniform binding sites. The two EIS electrochemical sensors were compared in terms of sensitivity and performance for the detection of E2. Binding behaviours anticipated that uniform binding sites indeed improved the sensor's performance.

EXPERIMENTAL SESSION

Chemicals

Acrylamide (Aam), N-*tert*-butylacrylamide (tBAm), methacrylic acid (MAA), N,N'-methylene bisacrylamide (BIS), N,N,N',N'-tetramethyl ethylenediamine (TEMED), ammonium persulfate (APS), β -estradiol, progesterone, bisphenol A (BPA), N-Cyclohexyl-2-aminoethanesulfonic acid (CHES), saline phosphate buffer (PBS), ethanol, sulfuric acid, sodium hydroxide, salt potassium ferrocyanide, Triton X-100 and were from Sigma-Aldrich (Merck KGaA, Darmstadt, Germany). Aniline was from Thermo Scientific (Thermo Fisher Scientific, Massachusetts, USA).

Synthesis of nanoMIPs and control NPs

The synthesis of the nanoMIPs was carried out using a total monomer concentration of 0.2% (w/v). The monomers used were 9.5 μ mol of Aam, 10.2 μ mol of MAA, 5.3 μ mol of tBAm and 103.7 μ mol of BIS, admixed in a volume of 10 mL of 20 mM PB at pH 7.4, supplemented of a sub-micellar concentration of SDS (0.01% w/v). The template, estradiol, was added in the polymerization solution at the final concentration of 1.28 mM. Vials were closed with rubber caps and bubbled with N₂ for 10 minutes. The catalysts, APS (0.04% w/v) and TEMED (0.03% w/v), were added and the polymerization was carried out overnight at room temperature under mild stirring. Non-imprinted polymers (control NPs) were synthesized with the same protocol without the addition of the template. At the completion of the polymerization of nanoMIPs the removal of the template was carried out by adding 2 mL of CHES free base 50 mM to obtain a solution with pH>9. Both nanoMIPs and control NPs were dialyzed against 1 litre of MilliQ water for 1 hour using a dialysis tubing with 14.000 MWCO (Sigma Aldrich, Milan, Italy). Then nanoparticles were dialyzed with 2 x 3 L of MilliQ water. Next, the nanoMIPs and control NPs were freeze-dried and stored. The yield of polymerization was 98% for the nanoMIPs and 96% for control NPs, as estimated from the weight of the lyophilized nanoparticles respect to the total weight of the monomers used in the synthesis.

Dynamic light scattering (DLS)

Size distribution and polydispersity index (PDI) were determined using a Zetasizer Nano ZEN3600 (Malvern Instruments Ltd, Worcestershire, UK) equipped with a 633 nm He-Ne laser at a detection angle of 173°. NanoMIPs were suspended in water to the final concentration of 1 mg/mL. The material refractive index (RI) was 1.490 and the absorption value 0.01; the dispersant RI was 1.332 for water, the viscosity was 0.89 cP as reported by the Zetasizer v.6.32 software (Malvern instruments Ltd, Worcestershire, UK). The temperature was set at 25°C. Measurements were in triplicate.

Electrochemical polymerization of PANI on gold electrodes

Electrochemical polymerizations were performed using a Palmsens4 potentiostat (Palmsens BV, Houten,

Netherlands) using a screen-printed gold electrode 220BT (Metrohm DropSense S.L., Llanera, Spain) with Au as working and auxiliary electrodes and an Ag as reference electrode. Before the electrochemical polymerization, to clean the sensor surface, electrodes were rinsed with deionised water and then a volume of 200 μL of H_2SO_4 0.25 M was placed on the electrodes and 3 scans of Cyclic Voltammetry (CV) were performed between -0.6 V and +0.5 V at a scan rate of 0.05 V/s. Prior to prepare electrodes, the electrochemical behaviour of E2 was investigated to confirm no contribution (SI Figure S1). For the electrochemical polymerization CV was performed between -0.5 V and +0.8 V for 15 cycles (SI Figure S2) at a scan rate of 0.05 V/s in a solution of aniline 0.025 M, previously diluted in H_2SO_4 0.25 M, in the presence of E2 at the final concentration of 660 μM to prepare the imprinted PANI layer and without E2 to prepare the PANI control layer. Both the imprinted PANI and PANI control were then subjected to a sequence of washing steps, carried out in the oven at a temperature of 40°C. Such steps consisted in dipping the electrodes in a solution of 75% NaOH 0.1 M and 25% of EtOH for 15 minutes, followed by an absolute EtOH solution for 5 minutes, with the whole process repeated twice. Then, the surface was blocked by placing a volume of 200 μL of PBS pH 5 supplemented with 0.05% Triton X-100 on the electrode for at 1 hour. The electrodes were washed with deionized water and dried.

Electrochemical Impedance Spectroscopy (EIS)

EIS, performed using the Palmsens4, was used to monitor changes at the electrode surface both during the preparation of the sensor (e.g., polymerisation, washing and blocking steps) and to assess rebinding in presence of increasing concentrations of E2. For the EIS measurements, a volume of 200 μL of 0.01 M $\text{Fe}(\text{CN})_6^{3-/4-}$ in PBS pH 5 was first placed on the electrode and incubated for 15 minutes to equilibrate. Then, the signal was recorded by setting a further equilibration time of 120 s, a 0.01 a.c. s and 0.12 d.c. voltages. The frequency varied from 0.1 Hz to 50000 Hz with 6.5 points impedance reading per decade. The impedance data were then represented in the form of Nyquist plots, which were fitted to an equivalent circuit (SI Figure S3) by the analysis function in PSTrace software (Palmsens BV, Houten, Netherlands) to extrapolate the charge-transfer resistance (Rct) values.

Electrochemical polymerization of PANI doped with nanoMIPs on gold electrodes

Electrodes were prepared as reported in 'Electrochemical polymerization of PANI on gold electrodes' section but using a solution of aniline 0.025 M, diluted in H_2SO_4 0.25 M, and supplemented with nanoMIPs (or control NPs) at the final concentration of 1 mg/mL.

After the electrochemical polymerization, electrodes were washed with deionized water and dried. To block the surface, a volume of 200 μL of PBS pH 5 supplemented with 0.1% Triton X-100 was placed on the electrodes for 1 hour. Then the electrodes were washed with deionized water and dried. The same protocol was used for the electrochemical polymerization of PANI doped with control NPs.

Scanning Electron Microscope (SEM)

SEM analysis was conducted using a Supra 40 Field Emission Microscope (Carl Zeiss AG, Oberkochen, Germany), collecting secondary electron emissions with a primary beam acceleration voltage of 2.5 kV.

FT-IR

FTIR spectra were obtained using a Spectrum Two FT-IR Spectrometer (Perkin Elmer, Massachusetts, USA), covering the spectral range from 400 to 4000 cm^{-1} with a resolution of 1 cm^{-1} .

Isothermal titration calorimetry (ITC)

Isothermal titration calorimetry (ITC) was performed on a Nano Isothermal Titration Calorimeter TA (TA instruments, New Castle, USA) instrument. All solutions were filtered and degassed prior to use. The nanoMIPs were solubilized in 10 mM PBS pH 7.4 at the final concentration of 2 mg/mL. Then, nanoMIP solution (230 μL) was titrated with E2 (3.6 μM , $V=50 \mu\text{L}$; 3 μL per injection) at 25° C, and the heats of the interactions were recorded in triplicate. Dilution heats were estimated from the titration of the E2 in buffer ($n=3$). Raw heats were subtracted from the dilution heats and integrated. Integrated heats were plotted as a function of the molar ratio between the titrand and the titrant and fitted with one set of sites modelled with the NanoAnalyze Software v. 3.4.0 (TA Instruments, New Castle, DE); according to manufacturer: $\text{Bound} = (-b - \sqrt{b^2 - 4 * a * c}) / (2 * a)$; $K_a \text{ value} = 1/K_d$; the quadratic constants a, b, and c were defined as follows: $a = K_a \text{ value}$; $b = -K_a \text{ value} * (\text{Mol_Syringe}(\text{iteration}) + \text{Mol_Cell}(\text{iteration}) * n) - \text{CellVolume}(\text{iteration} / 1e6)$; $c = K_a \text{ value} * \text{Mol_Syringe}(\text{iteration}) * \text{Mol_Cell}(\text{iteration}) * n$. The enthalpy (ΔH°) was calculated from $\text{Heat} = 1e9 * (\text{Bound} - \text{Old bound}) * dh$; and free energy variation (ΔG°) were calculated from K_D and ΔH° .

Estradiol re-binding

For the E2 rebinding experiments, a volume of 200 μL of PBS was supplemented with H_2SO_4 to pH 5, without E2 (0) first and then with increasing concentrations of E2 (from 0.01 ng/mL to 500 ng/mL). Each solution was placed on the electrode for 30 minutes followed by washing with deionized water. EIS measurements and data fitting were then carried out after each analyte concentration as explained in the 'Electrochemical Impedance Spectroscopy' section. The Rct values recorded for each concentration were then normalised using the following formula:

$$\text{Norm. Rct} = \frac{Rct_x - Rct_0}{Rct_0} \quad (1)$$

Sensor's parameters

Normalized Rct values, plotted as a function of E2 concentration, were fitted with Langmuir (eq. 2) and Hill (eq. 3) equation models (OriginPro 9.0):

$$R_{ct} = R_{ct,max} \frac{x}{(K + x)} \quad (2)$$

$$R_{ct} = R_{ct,max} \frac{x^n}{(K + x^n)} \quad (3)$$

Where R_{ct} is the impedance at concentration x of the ligand (i.e. [E2]); $R_{ct,max}$ is the R_{ct} value at binding saturation; n is the Hill parameter, that correlates with the number of binding sites, and K is the apparent dissociation constant derived from the mass law action.

Cross-reactivity studies

The selectivity of both imprinted PANI and PANI doped-nanoMIPs electrodes was tested in EIS using two analogues, bisphenol A and progesterone, at three different concentrations (0.1, 1 and 50 ng/mL). Re-biding of analogues was done in the same way as re-biding of E2 and the EIS measurements were performed as reported in the "Electrochemical Impedance Spectroscopy (EIS)" paragraph.

Wastewater sample collection

The wastewater sample (1 L) was collected from the outlet of the wastewater treatment tank of the UKCRIC National Research Facilities for Water and Wastewater Treatment situated at Cranfield University. Immediately after collection, the sample was transferred to the laboratory, aliquoted in 50 mL falcon tubes and these stored at -20°C until use.

Real sample analysis

Both imprinted PANI and PANI doped-nanoMIPs electrodes were tested with the wastewater sample, spiked with increasing concentrations of estradiol (0.1, 1 and 50 ng/mL). Specifically, the wastewater sample was spiked with estradiol either before or after filtration with a $0.45\ \mu\text{m}$ PTFE filter (Corning Incorporated, New York, USA) and diluted 1:1 with phosphate buffer supplemented with a solution of H_2SO_4 (pH 5). A volume of $200\ \mu\text{L}$ of the spiked sample was then placed on the electrodes and, after 30 minutes of incubation, EIS measurements were performed as described in the paragraph Electrochemical Impedance Spectroscopy (EIS).

Statistical analysis

Data significance was evaluated by performing a one-way ANOVA test with post-hoc Tukey HSD using the online tool provided at <https://astatsa.com>.

Computational details

Density Functional Theory (DFT) simulations were carried out with the ORCA Software, Version 5.0.3.²⁸⁻³⁰ Geometry optimization of the monomer-estradiol adducts were performed with the RIJCOSX approximation³¹ and employing the B3LYP exchange-correlation functional,³² a def2-SVP together with the auxiliary def2/J basis sets, and D3BJ to take into account dispersion interactions.

RESULTS AND DISCUSSION

Rational selection of the monomers

Molecular modelling by means of Density Functional Theory (DFT) was used to estimate the theoretical strength of the interaction between monomers and template as a method that to rationally select the best monomer composition for the imprinting processes.³³ The monomer composition is pivotal for generating stable pre-polymerization complexes in solution, thus fixing the binding cavity's stereochemistry, ultimately favouring highly selective MIPs. Here, we compared the interaction energy between E2 and its imprinted PANI layer, which epitomized the condition of continuum of binding sites, against the interaction energy between E2 and polyacrylamide's nanoMIPs, prepared by means of a standard monomers mixture composition,³⁴ which epitomized discrete homogeneous binding sites. Therefore, the molecular interactions between E2 and aniline or E2 and each functional monomer used for the synthesis of the nanoMIPs are reported in Figure 2. The interaction energies (ΔE) for the pairs E2/aniline and for E2/acrylamides were calculated from the energy difference between the pair and the isolated E2 and template molecules, resulting in a ΔE of $-12.45\ \text{kcal/mol}$ for aniline, while this further lowered to -36.14 , -17.37 and $-15.00\ \text{kcal/mol}$ for the deprotonated MAA, Aam, and *t*BAm, respectively, suggesting more stabilizing interactions in the case of the acrylamide derivatives.

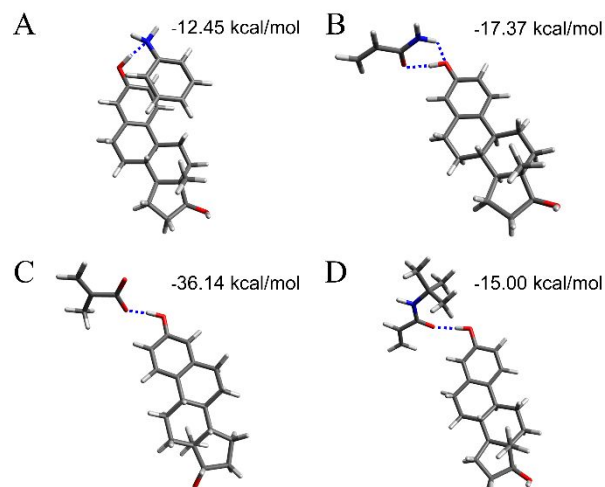


Figure 2. Molecular modelling. Sketches of the interaction between E2 and the monomers: Aniline (A), that is the monomer used to prepare the imprinted-PANI layer, and the functional monomers used for the synthesis of the nanoMIPs, that are Acrylamide (B), Methacrylic acid (C) and *tert*-butylacrylamide (D).

The Imprinted PANI EIS Sensor

An E2 imprinted PANI EIS sensor was prepared, and its behaviour was studied. For the preparation of the electrode, aniline was electrochemically polymerized in the presence of the template (660 nmol of E2). The polymerization was carried out in an aqueous solution in strong oxidizing

protonic acid H_2SO_4 , using potentiodynamic electrochemical polymerization by cycling the potential between -0.5 V and $+0.8\text{ V}$ at a potential scan rate of 0.02 V/s for 15 cycles and with Ag pseudo reference. Figures 3A and 3B show the current-potential curves of potentiodynamic electropolymerization of aniline respectively in the presence of the E2 template, that is referred to as imprinted PANI layer, and in the absence of E2, defined as PANI control. The anodic peaks at 0.1 V , present in the imprinted PANI layer, and in PANI control, were assigned to irreversible electro-oxidation of aniline. The peaks were observed growing up to $n=15$ CV scans (details in SI), confirming a successful polymerization of aniline and indicating the formation of a conducting thin film.³⁵ It was observed that the maximum current peak at 0.1 V in the case of PANI control was higher with respect to that of the imprinted PANI layer, indicating that a thicker PANI layer was deposited in the absence of the template.

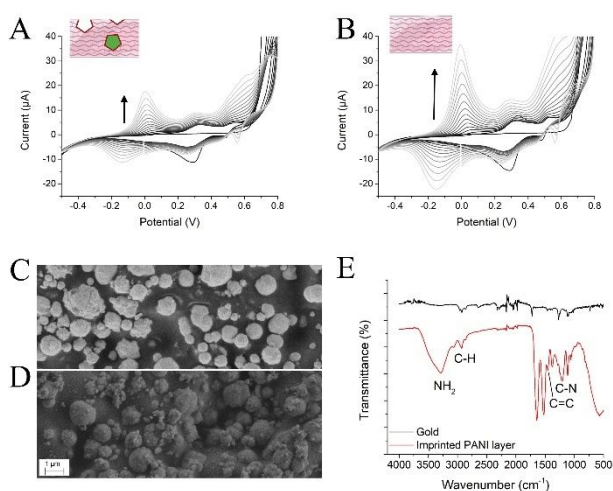


Figure 3. CV of Imprinted PANI layer (A) and of PANI control (B). SEM image of bare electrode (C) and Imprinted PANI layer (D) FT-IR spectra (E).

Subsequently, the template was extracted using 75% NaOH 0.1 M and 25% of EtOH followed by a step in absolute ethanol to disrupt both the electrostatic and hydrophobic interactions. To avoid non-specific interactions, both control and imprinted PANI modified electrodes were blocked with a solution of PBS pH 5 supplemented with 0.1% Triton X-100. After equilibrating the pH of the electrodes by incubating them with a drop of 200 µL of PBS pH 5 for 1 hour, the template extraction and the blocking steps were monitored with EIS measurements (details in SI). The Nyquist plots of the imprinted PANI layer (SI Figure S4A) showed a reduction of the charge transfer resistance R_{ct} (bare electrode: $150\ \Omega$, PANI electrode: $34\ \Omega$) associated with the electropolymerization of aniline, while the R_{ct} increased after template removal and blocking (after blocking: $300\ \Omega$). The increase of R_{ct} after washing (and equilibration at pH 5.0) can be attributed to the decrease in conductivity of polyaniline as the pH rise from the highly acidic environment in which the film was formed ($0.25\text{ M H}_2\text{SO}_4$). The further increase after blocking is due to

the successful deposition of an additional layer of the non-conductive surfactant (Triton-X) that reduces further the overall conductivity of the electrode, increasing the charge-transfer resistance.

PANI control electrodes were prepared and treated in the same manner as the imprinted PANI and showed a similar electrochemical behaviour (SI Figure S4B).

PANI modified electrodes, both imprinted and controls, were next physically characterized. SEM images evidenced the polymer layer (Figure 3D) at the surface of bare gold electrode (Figure 3C), as a finer structure deposited over the globular gold surface. FT-IR spectra of the PANI film (Figure 3E, red line) compared with that of bare gold electrode (Figure 3E, black line), showed specific IR bands corresponding to N-H bond vibrations (3200 cm^{-1}), C-H vibrations ($2921, 1373\text{ cm}^{-1}$), C=N (1650 cm^{-1}), C=C ($1515, 1450\text{ cm}^{-1}$) and C-N (1255 cm^{-1}), thus confirming the deposition of the PANI layer onto the gold SPE.³⁶

The ability of the imprinted PANI layer electrode to rebind E2 was tested and compared with the PANI control electrode. Rebinding studies were performed using concentrations of E2 ranging from 0.01 to 100 ng/mL, as shown in Figure 4. It can be observed that imprinted PANI layer sensor (Figure 4A) showed EIS signals with R_{ct} values increasing proportionally to the concentration of E2 (from $342\ \Omega$ - $455\ \Omega$), indicating the successful binding of a non-conductive molecule on the polyaniline. In contrast, when PANI control sensor was tested, it did not show changes in the EIS signal upon E2 addition (Figure 4B). The normalized data of R_{ct} obtained from the EIS measurements of the imprinted PANI layer and control and calculated as explained in the 'Estradiol rebinding' section, were plotted as a function of E2 concentrations (Figure 4C). It can be observed, that normalized R_{ct} for control PANI did not report any binding event, whereas characteristics saturation binding isotherms were observed for the imprinted PANI layer.

Data of the imprinted PANI layer were fitted with the Langmuir isotherm equation (Figure 4D), which is meant to describe monomodal binding sites ($n=1$). The sensor's half saturation was estimated with an $EC_{50} = 0.0722\text{ ng/mL}$, but the fitting was quite poor, considering the $R^2=0.8863$ value (Table 1). This suggested that the process of imprinting the E2 soluble template through PANI electropolymerization yielded to heterogeneous stamping of the binding sites, as also theorized by Umpleby II.¹³ Then, the same set of data was fitted with a Hill model equation (Figure 4E), which extends the liberty degree for the binding sites to n . The value of EC_{50} resulted 0.1434 ng/mL , $n = 0.34$, and $R^2=0.9934$ (Table 1). Taking n as an approximation of the heterogeneity of the surface binding sites, the results suggested that the imprinted PANI layer possessed inhomogeneous binding cavities.

The overall operational parameters of the imprinted PANI layer-sensor indicated that the electrode could be exploited to determine E2 in the picomolar range. Figure 3F shows the linear correlation plot between normalized R_{ct} and the concentrations of E2. The linear regression equation was: $y(R_{ct}) = 0.2432 + x\left(\frac{\text{ng}}{\text{mL}}\right)0.0673$ ($R^2=$

0.9982) (Table 1) with a LOD of 65.04 pg/mL and a sensitivity at low concentration of 2.60 ng/mL (Table 3).

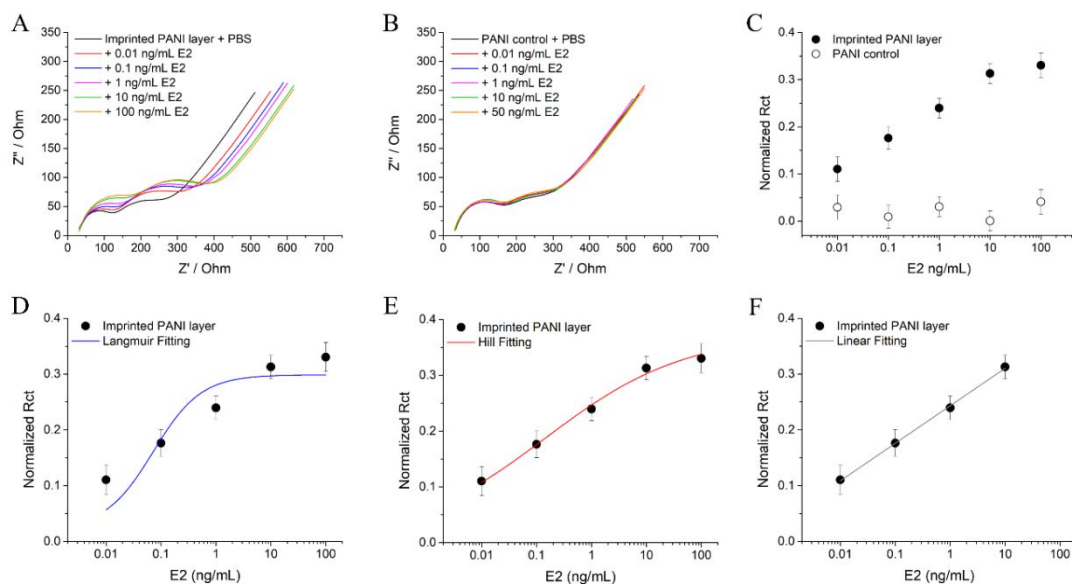


Figure 4. Nyquist plot of Imprinted PANI layer (A) and of PANI control (B) incubated with increasing concentrations of E2. Normalized Rct as function of E2 concentrations of Imprinted PANI layer and PANI control (C). Imprinted PANI layer fitted with Langmuir (D), Hill (E) and Linear (F) equation models.

Table 1. Fitting Parameters Imprinted PANI layer.

Fitting	Rct_min	Rct_max	EC ₅₀ (ng/mL)	n	Intercept	Slope	Statistics	
							R ²	χ ²
Langmuir	0.0233 ± 0.0790	0.2988 ± 0.0282	0.0722 ± 0.0761	1	/	/	0.8863	3.8406
Hill	0.0003 ± 0.1620	0.3740 ± 0.0565	0.1434 ± 0.3003	0.3402 ± 0.2203	/	/	0.9934	0.2229
Linear	/	/	/	/	0.2433 ± 0.0018	0.0673 ± 0.0016	0.9982	/

The nanoMIPs-doped PANI EIS Sensor

In the second part of the work, an EIS sensor based on discrete and homogeneous binding sites was studied. Electrodes were modified with a PANI layer, to which the selective recognition was entailed by doping it with E2-selective nanoMIPs, and supposedly playing the role of homo-binding cavities (Figure 1B). The performances of two sensors were ultimately compared.

NanoMIPs were synthesized using a total monomer concentration of 0.2% w/v.³⁴ Acrylamide (Aam), *tert*-butylacrylamide (*t*BAm), and methacrylic acid (MAA) were admixed to *N,N'*-methylene bis-acrylamide (BIS), which was used as a reticulating agent. E2 (1.28 mM) was chosen as a

template and added to the pre-polymerization mixture ($V_{\text{final}} = 10$

mL). The nanoMIPs dimensions were characterized by means of dynamic light scattering (DLS; SI Figure S5). The hydrodynamic sizes of the nanoparticles were about a few hundreds of nanometers, while the polydispersity index (PDI) indicated a homogeneous distribution (SI Table S1). The functional characterization of nanoMIPs was assessed by isothermal titration calorimetry (ITC). Figure S6 reports the interaction between the nanoparticles and E2, subtracted of the non-specific heats, measured by the interaction of E2 with control non-imprinted nanoparticles

(control NPs). The integrated heats described a sigmoidal profile typically associated with interacting molecules. Binding data were fit with an independent equation model, showing a dissociation constant of 11 nM and a single binding site per nanoMIP (details in SI Figure S6; SI Table S2). Thus, the ITC confirmed the effective stamping of binding sites on the nanoMIPs.

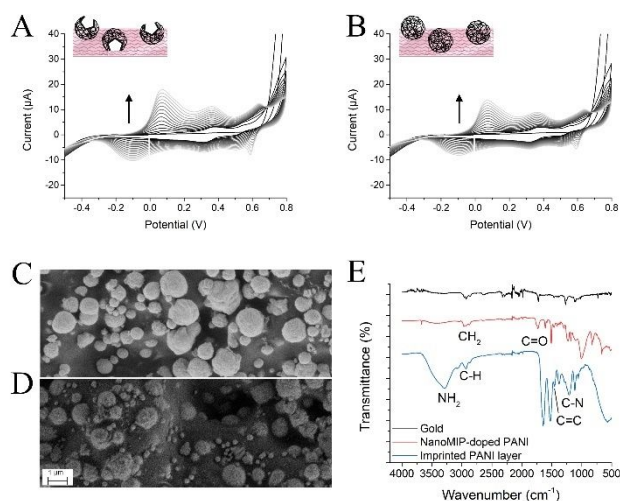


Figure 5. CV of nanoMIP-doped PANI (A) and of control NPs-doped PANI (B). SEM image of bare electrode (C) and of nanoMIP-doped PANI (D) FT-IR spectra (E).

For the preparation of the electrodes, aniline was electrochemically polymerized in the presence of nanoMIPs or of control NPs. The polymerization was carried out in the same conditions reported for the imprinted PANI layer. Figures 5A and 5B show the current–potential curves of potentiodynamic electropolymerization of aniline in the presence of nanoMIPs (nanoMIPs-doped PANI) and in the presence of control NPs (control NPs-doped PANI), respectively. The anodic peak at 0.1 V, present in both nanoMIPs-doped PANI and control NPs-doped PANI, was assigned to irreversible electro oxidation of the aniline. The peak was observed growing up to $n=15$ CV scans (details in SI), confirming the polymerization of aniline and indicating the formation of a conducting thin film, in analogy to what reported earlier. Subsequently, electrodes were blocked with a solution of PBS pH 5 supplemented with 0.1% Triton X-100 to avoid non-specific interactions.

The surface of the electrode was imaged by SEM as reported in Figure 5C and, confirmed the presence of a polymeric layer after modification of the gold SPE with nanoMIP embedded in PANI, similarly to what reported in Figure 3. Yet, FT-IR spectra of nanoMIP-doped PANI (Figure 3E, red line) showed the typical bands associated to polyacrylamide, thus confirming the incorporation of nanoMIPs at the electrode surface. In particular, the peaks at 2923 cm⁻¹, at 1659 cm⁻¹ and at 1119 cm⁻¹ are associated with the -CH₂ stretching vibrations, C=O stretching vibrations and C-N bond, respectively.³⁷ Moreover, in the nanoMIP-doped PANI FT-IR spectrum there were bands typical of PANI, suggesting the electropolymerization had occurred. Typically, we reported the peak associated to the

N-H bond vibrations (3200 cm⁻¹), C-H vibrations (2921, 1373 cm⁻¹), C=C (1515, 1450 cm⁻¹) and C-N (1255 cm⁻¹).

Figure 6 shows the EIS measurements of nanoMIPs-doped PANI and the control NPs-doped PANI after incubation with concentrations of E2 ranging from 0.01 ng/mL to 500 ng/mL. The obtained Nyquist plots in Figure 6A demonstrated that increasing E2 concentrations led to an increase in the impedimetric responses of the nanoMIPs-doped PANI sensor, suggesting the formation of bonds between the selective binding cavities on the nanoMIPs and the non-conductive E2 analyte. The E2 to nanoMIP interaction served as a kinetic barrier, inhibiting the transfer of electrons between the sensor surface and the sensing probe in solution, resulting in enhancement of Rct (from 105 Ω to 305 Ω). In contrast, the control NPs-doped PANI sensor, used as a negative control, did not show changes in the EIS signal upon E2 addition.

The normalized Rct data obtained from the EIS measurements of nanoMIPs-doped PANI and control NPs-doped PANI were plotted as a function of E2 concentration (Figure 6C). Characteristics saturation binding isotherms were observed for nanoMIPs-doped PANI, whereas control NPs doped PANI did not report any response to binding events. Langmuir model equation (Figure 6D) was employed to fit the data of the binding isotherm, showing an EC₅₀ of 0.5354 ng/mL and an R² = 0.9690 when the binding site density n was equal to 1. Whereas Figure 6E reports the fitting made with the Hill equation model, that estimated an EC₅₀ of 0.6440 ng/mL, $n = 0.79$, R² = 0.9955.

The n parameter, which inversely correlates to the degree of heterogeneity of the binding sites (i.e. homogeneous for $n=1$), was much closer to the unit for nanoMIP-doped PANI ($n=0.79$) as compared with the imprinted PANI layer ($n=0.34$). This observation reinforces the hypothesis that nanoMIPs can act as discrete and homogeneous binding sites. Yet, the n value for the nanoMIP-doped PANI was not exactly 1, possibly due to influences from non-specific interactions and from the orientations of nanoMIPs dispersed in the PANI layer, that were assumed to yield to on/off binding sites only (Figure 1B), while being more multifaceted. However, despite possible inaccuracies of the model, the n values and the related statistics for nanoMIP-doped PANI compared with imprinted PANI layer, fully supporting the effect of nanoMIPs as homogeneous sites (Table 1). This can be taken as a general descriptor of sensors where nanoMIPs play the role of discrete homogeneous receptors. In fact, in the literature there are examples that reports the sensing of the cardiac troponin I, marker for myocardial infarction, with a nanoMIP-receiving layer that yielded to binding isotherms best fitted with a Langmuir model ($n=1$) and an R²=0.99, in contrast to the fit values obtained for a Langmuir-Freundlich model, that were $n=0.26$ and R²=0.89.³⁸ Another study reports the determination of cilostazol and its pharmacologically active primary metabolite in human plasma and was performed by means of a nanoMIP chemosensor.³⁹ The nanoMIP chemosensor was prepared embedding cilostazol-selective nanoMIPs in a poly-tyramine layer. Isotherm's parameters for the nanoMIP chemosensor curves of normalized DPV peak current versus the cilostazol concentrations, showed that Langmuir model ($n=1$) had an R²=0.959, Freundlich

showed a $n=4.04$ but a poorer $R^2=0.86$, Langmuir-Freundlich model showed $n=1.02$ and $R^2=0.949$, suggesting that the nanoMIPs indeed behave as homogeneous binding sites.

From Figure 6 the operational parameters of the E2 nanoMIPs-doped PANI sensor were estimated. The sensor could be exploited to determine E2 in the nanomolar range.

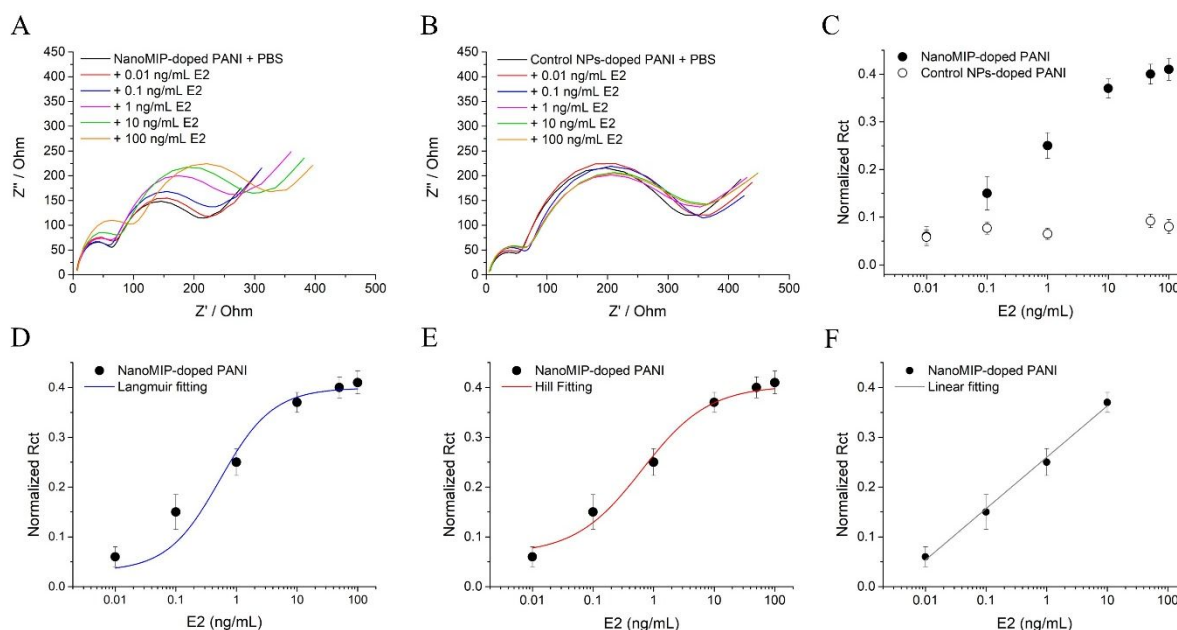


Figure 6. Nyquist plot of nanoMIP-doped PANI (A) and of control NP-doped PANI (B) incubated with increasing concentrations of E2. Normalized Rct as a function of E2 concentration of nanoMIP-doped PANI and control NP-doped PANI (C). NanoMIP-doped PANI fitted with Langmuir (D), Hill (E) and Linear (F) equation model.

Table 2. Fitting parameters of nanoMIP-doped PANI.

Fitting	Rct_min	Rct_max	EC ₅₀ (ng/mL)	n	Intercept	Slope	Statistics	
							R ²	χ ²
Langmuir	0.0307 ± 0.0304	0.3991 ± 0.0188	0.5354 ± 0.2695	1			0.9690	1.9236
Hill	0.0655 ± 0.0006	0.4038 ± 0.0005	0.6443 ± 0.0078	0.79 ± 0.09			0.9955	0.00006
Linear					0.2598 ± 0.0057	0.1031 ± 0.0046	0.9940	

Table 3. Operational parameters associated to Imprinted PANI layer and nanoMIP-doped PANI sensors.

	Imprinted PANI layer	nanoMIP-doped PANI
Rct_min	0.0003 ± 0.162	0.0655 ± 0.0006
Rct_max	0.3740 ± 0.0565	0.4038 ± 0.0005
K _{app} (M)	5.14×10 ⁻¹⁰	2.37×10 ⁻⁹
K _{aff} (M ⁻¹) ^a	1.95×10 ⁹	4.23×10 ⁸
LOD (pg/mL) ^b	65.04	2.86

Sensitivity at low concentrations ^c

2.606

0.525

$$a = \frac{1}{K_{app}}; b = \frac{(3 \times St.Dev.blank)}{Sensitivity\ at\ low\ conc.}; c = \frac{\Delta Rct}{K_{app}}$$

Figure 6F showed the linear correlation plot between normalized Rct and the logarithm of E2 concentrations. As reported in Table 2, the regression equation normalized was $y = 0.2598 + x 0.103$ ($R^2 = 0.9940$) with a LOD of 2.86 pg/mL and a sensitivity at low concentration of 0.525 ng/mL (Table 3). Table 3 reports the comparison between the performance parameters of the imprinted PANI layer and the nanoMIP-doped PANI. It can be observed that both sensors exhibited a response for E2 in the range 36.7 pM-36.7 nM, indicating a superior sensitivity respect to other MIP-electrodes in the literature.²¹ Particularly interesting are the linearization parameters (i.e. compare Figure 4F and Figure 6F), where the slope for the imprinted PANI layer was $0.058 \Omega/ng\ ml^{-1}$, whereas the slope for the nanoMIP-doped PANI was $0.103 \Omega/ng\ ml^{-1}$. A gain of almost twice the sensitivity was therefore achieved for a sensing surface provided of discrete homogeneous binding sites, respect to when the binding sites were inhomogeneously stamped in the PANI layer.

Selectivity

To test the selectivity of both imprinted PANI layer and nanoMIPs-doped PANI sensor, the electrode responses were assessed by choosing as interferences other two common water contaminants with structural similarity to E2: Bisphenol A and Progesterone (SI, Figure S7). The interferences were added independently at the concentrations of 0.1, 1 and 50 ng/mL in PBS and the EIS measurements were taken after 30 min of incubation and a quick washing with water. The EIS quantifications were executed in three replicates, and the outcomes are depicted in the histograms reported in Figure 7. The responses for each interference were compared to that of the E2. As appeared in Figure 7A, it was clear that the Rct value of the imprinted PANI layer sensor towards E2 was higher than that of the potential interferences, demonstrating selectivity for E2. Similar behaviour can be observed for nanoMIPs-doped PANI electrodes (Figure 7B). NanoMIPs on the electrode presented high selectivity and unique recognition ability toward E2.

Reproducibility

The reproducibility of the Imprinted PANI layer and nanoMIP-doped PANI electrodes was investigated by detecting the concentration of E2 (0.1 and 1 ng/mL), respectively on three and on five electrodes, prepared in the same conditions. Figure 8 reports the normalized Rct value of the five nanoMIP-doped PANI electrodes (Figure 8A) and the three Imprinted PANI layer electrodes (Figure 8B). The relative standard deviations (RSD) reported in Table 4 were calculated for both nanoMIP-doped PANI and Imprinted PANI layer electrodes. The RDS of nanoMIP-doped PANI was significantly lower with respect to that of Imprinted

PANI layer, indicating high sensor-to-sensor reproducibility when the PANI layer is doped with nanoMIPs.

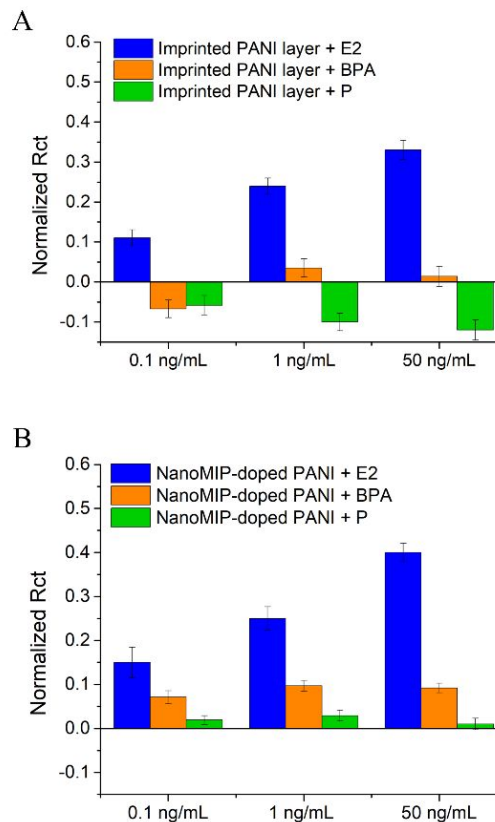


Figure 7. Normalized Rct of Imprinted PANI layer (A) and nanoMIP-doped PANI (B) incubated with E2 (blue bar), BPA (orange bar) and P (green bar) at different concentrations.

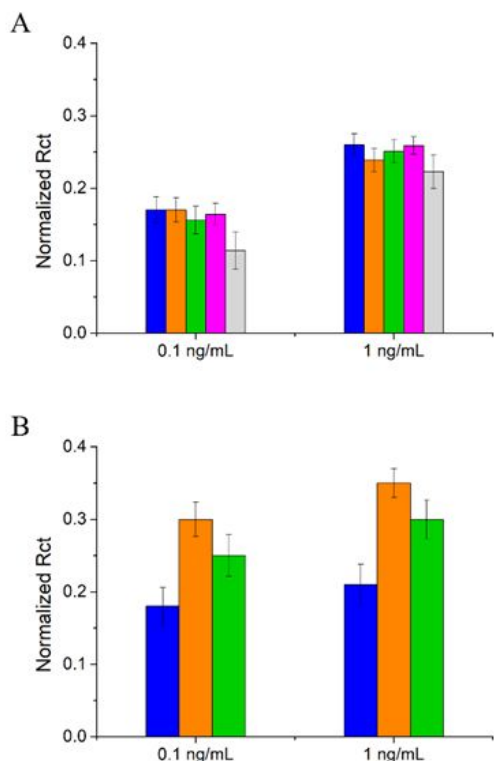


Figure 8. Reproducibility of nanoMIPs-doped PANI (A) and of Imprinted PANI layer (B).

Table 4. Relative standard deviation (RSD).

E2 (ng/mL)	nanoMIP-doped PANI	Imprinted PANI layer
0.1	15.194	24.771
1	6.311	24.749

NanoMIPs-doped PANI electrode for the detection of E2 in wastewater sample

At last, the nanoMIPs-doped PANI sensor was tested for its response in real scenarios samples, for the determination of E2 contamination in wastewaters. Real wastewater samples were spiked with known concentrations of E2, namely 0.1, 1 and 10 ng/mL and measured with the nanoMIP-doped PANI sensor. Additionally, to assess the effect on the measurement of sample treatment, wastewater samples were either spiked with E2 before or after filtration (i.e. to remove particulates) with 0.45 μm filters. All spiked wastewater samples were incubated for 30 minutes on the electrodes and next measured by EIS. Figure 9 reports the normalized Rct as a function of the E2 spiked in the wastewater samples. The Rct values increased for increasing E2 concentrations, alike the results obtained with E2 in PBS (SI Table S3).

Normalized Rct of E2 in buffer (Figure 9 blue squares) was used as a reference curve. Measurements of E2 in filtered wastewater (Figure 9 red circles) well overlapped with PBS data, with no statistical differences calculated at 0.1 ng/mL and 1 ng/mL (p-values equal to 0.058 and 0.06, respectively) and moderate statistical difference at 10 ng/mL (p=0.03). Wastewater samples spiked with E2 prior to filtration (Figure 9 black triangles) instead showed a significant variation of the normalized Rct values respect to buffer, suggesting that the filtration step might yield to partial non-specific sorption of E2 on the filter.

When the recoveries of E2 in spiked wastewater samples were calculated, these resulted to be 98.7%, 96.9% and 68.7% respectively for the addition of E2 at the concentrations of 0.1, 1 and 10 ng/mL.

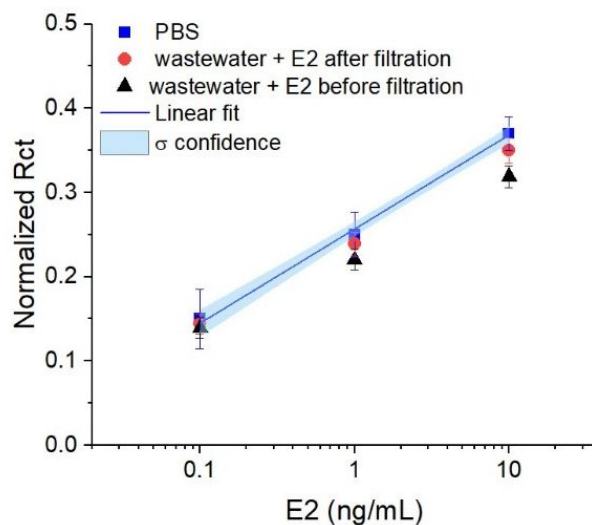


Figure 9. Normalized Rct as a function of E2 concentration of the EIS-nanoMIP-doped PANI sensor incubated with wastewater spiked with different concentrations of E2 before filtration (black triangles), or after filtration (red dots) compared to the E2 measurements in PBS (blue squares); linear fit of E2 in PBS $y=0.111x + 0.256$ (blue line); light blue halo represents the 1 σ confidence level for the fitting.

CONCLUSIONS

MIPs are considered ideal receptor elements for sensing devices, given the possibility to custom-design their selectivity, their affinity towards a targeted analyte and their robustness, that enable them to withstand harsh conditions. However, MIP synthesis, even in the case of the electropolymerization of MIP thin films, is a random process that produces a statistical distribution of binding sites, with a variety of affinities, which might affect the sensor performance. With the aim to investigate the possible implications on the efficiency of the electrochemical sensor's performance of inhomogeneous imprinted binding sites formed at the surface of the working electrode, we simulated two different scenarios. On one side, we prepared an electrode onto which an E2 imprinted PANI layer was electro-deposited, and we compared it with the performance of a PANI layer doped

with E2-selective nanoMIPs, these latter intended as a model of homogeneous and discrete binding sites.

Studying the binding behaviour of the two sensors towards their analyte, the hormone E2, through the EIS technique, confirmed that the direct imprinting of E2 in the PANI layer allowed forming heterogeneous binding sites. In contrast, E2-selective nanoMIPs embedded in an electropolymerized PANI layer provided homogeneity of the binding sites, with the key advantage of improving almost twice the sensitivity of the sensor. These results indicate that the quality of the binding sites should play a fundamental role in sensor development.

ASSOCIATED CONTENT

Supporting Information. File name: SI_Marinangeli.pdf. Content: Investigation of electrochemical behaviour of E2; CVs of electrodeposition of aniline for imprinted PANI electrode and nanoMIPsdoped PANI electrode; Fitting PSTrace software; Preparation of imprinted PANI layer and PANI control; DLS of nanoMIPs; ITC of nanoMIPs; Structure of interferents; Real sample measurements.

AUTHOR INFORMATION

Corresponding Author

*Alessandra Maria Bossi, Department of Biotechnology, University of Verona, Strada Le Grazie 15, 37134 Verona, Italy. E-mail: alessandramaria.bossi@univ.it

Author Contributions

Conceptualization, A.M., I.C. and A.M.B.; methodology, A.M., I.C., E.R. and D.M.; validation, A.M.; investigation, A.M., D.M. and E.R.; resources, A.M.B.; data curation, A.M., A.M.B.; writing—original draft preparation, A.M., A.M.B.; writing—review and editing, A.M., I.C., D.M. and A.M.B.; supervision, A.M.B. and I.C. The manuscript was written through contributions of all authors. / All authors have given approval to the final version of the manuscript. / ‡These authors contributed equally.

Funding Sources

Italian Ministry of Research and University doctoral program PON PNRR D.M.351.

ACKNOWLEDGMENT

A.M.B. and A.M. acknowledge Ministry of University and Research for MUR D.M. 351 PON PNRR doctoral program. A.M.B. acknowledges the Centro Piattaforme Tecnologiche (CPT) of the University of Verona for the facilities DLS and ITC.

ABBREVIATIONS

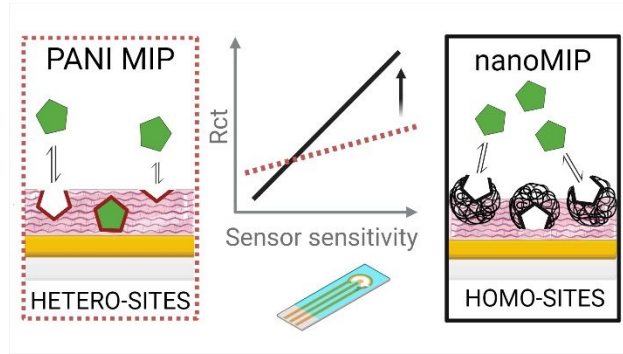
MIP, molecularly imprinted polymer, PANI, polyaniline, SPE, screen-printed electrode, EIS, electrochemical impedance spectroscopy, DPV, differential pulse voltammetry, CV, cyclic voltammetry, DLS, dynamic light scattering, SEM, scanning electron microscopy, ITC, isothermal titration nanocalorimetry, LOD, limit of detection, PDI, polydispersity index, RI, refractive index, RSD, relative standard deviation.

REFERENCES

- Wulff, G.; Sarhan, A.; Zabrocki, K. Enzyme-Analogue Built Polymers and Their Use for the Resolution of Racemates. *Tetrahedron Lett.* **1973**, *14*, 4329–4332, doi:10.1016/S0040-4039(01)87213-0.
- Arshady, R.; Mosbach, K. Synthesis of Substrate-Selective Polymers by Host-Guest Polymerization. *Makromol. Chem.* **1981**, *182*, 687–692, doi:10.1002/MACP.1981.021820240.
- Wei, S.; Mizaikoff, B. Binding Site Characteristics of 17 β -Estradiol Imprinted Polymers. *Biosens. Bioelectron.* **2007**, *23*, 201–209, doi:10.1016/J.BIOS.2007.03.031.
- Rushton, G.T.; Karns, C.L.; Shimizu, K.D. A Critical Examination of the Use of the Freundlich Isotherm in Characterizing Molecularly Imprinted Polymers (MIPs). *Anal. Chim. Acta* **2005**, *528*, 107–113, doi:10.1016/J.ACA.2004.07.048.
- Malitesta, C.; Mazzotta, E.; Picca, R.A.; Poma, A.; Chianella, I.; Piletsky, S.A. MIP Sensors - The Electrochemical Approach. *Anal. Bioanal. Chem.* **2012**, *402*, 1827–1846, doi:10.1007/S00216-011-5405-5.
- Wang, L.; Zhang, W. Molecularly Imprinted Polymer (MIP) Based Electrochemical Sensors and Their Recent Advances in Health Applications. *Sens. Actuators Reports* **2023**, *5*, 100153, doi:10.1016/J.SNR.2023.100153.
- Lahcen, A.A.; Amine, A. Recent Advances in Electrochemical Sensors Based on Molecularly Imprinted Polymers and Nanomaterials. *Electroanalysis* **2019**, *31*, 188–201, doi:10.1002/ELAN.201800623.
- Ayerdurai, V.; Cieplak, M.; Kutner, W. Molecularly Imprinted Polymer-Based Electrochemical Sensors for Food Contaminants Determination. *Trends Anal. Chem.* **2023**, *158*, 116830, doi:10.1016/J.TRAC.2022.116830.
- Stojanovic, Z.; Erdőssy, J.; Keltai, K.; Scheller, F.W.; Gyurcsányi, R.E. Electrosynthesized Molecularly Imprinted Polyscopoletin Nanofilms for Human Serum Albumin Detection. *Anal. Chim. Acta* **2017**, *977*, 1–9, doi:10.1016/J.ACA.2017.04.043.
- Palladino, P.; Bettazzi, F.; Scarano, S. Polydopamine: Surface Coating, Molecular Imprinting, and Electrochemistry-Successful Applications and Future Perspectives in (Bio)Analysis. *Anal. Bioanal. Chem.* **2019**, *411*, 4327–4338, doi:10.1007/S00216-019-01665-W.
- Pirzada, M.; Sehat, E.; Altintas, Z. Cancer Biomarker Detection in Human Serum Samples Using Nanoparticle Decorated Epitope-Mediated Hybrid MIP. *Biosens. Bioelectron.* **2020**, *166*, doi:10.1016/J.BIOS.2020.112464.
- Kushwaha, A.; Srivastava, J.; Singh, A.K.; Anand, R.; Raghuvanshi, R.; Rai, T.; Singh, M. Epitope Imprinting of Mycobacterium Lepae Bacteria via Molecularly Imprinted Nanoparticles Using Multiple Monomers Approach. *Biosens. Bioelectron.* **2019**, *145*, doi:10.1016/J.BIOS.2019.111698.
- Umpleby, R.J.; Baxter, S.C.; Chen, Y.; Shah, R.N.; Shimizu, K.D. Characterization of Molecularly Imprinted Polymers with the Langmuir-Freundlich Isotherm. *Anal. Chem.* **2001**, *73*, 4584–4591, doi:10.1021/AC0105686.
- Pap, T.; Horvai, G. Binding Assays with Molecularly Imprinted Polymers—Why Do They Work? *J. of Chromatogr. B* **2004**, *804*, 167–172, doi:10.1016/J.JCHROMB.2003.12.007.
- Drzazgowska, J.; Schmid, B.; Sussmuth, R.D.; Altintas, Z. Self-Assembled Monolayer Epitope Bridges for Molecular Imprinting and Cancer Biomarker Sensing. *Anal. Chem.* **2020**, *92*, 4798–4806, doi:10.1021/ACS.ANALCHEM.9B03813.

16. deCatanzaro, D. Sex Steroids as Pheromones in Mammals: The Exceptional Role of Estradiol. *Horm. Behav.* **2015**, *68*, 103–116, doi:10.1016/J.YHBEH.2014.08.003.
17. Shore, L.S.; Shemesh, M. Estrogen as an Environmental Pollutant. *Bull. Environ. Contam. Toxicol.* **2016**, *97*, 447–448, doi:10.1007/S00128-016-1873-9.
18. Nazari, E.; Suja, F. Effects of 17 β -Estradiol (E2) on Aqueous Organisms and Its Treatment Problem: A Review. *Rev. Environ. Health* **2016**, *31*, 465–491, doi:10.1515/REVEH-2016-0040.
19. Wang, J. Portable Electrochemical Systems. *Trends Anal. Chem.* **2002**, *21*, 226–232, doi:10.1016/S0165-9936(02)00402-8.
20. Luo, X.; Morrin, A.; Killard, A.J.; Smyth, M.R. Application of Nanoparticles in Electrochemical Sensors and Biosensors. *Electroanalysis* **2006**, *18*, 319–326, doi:10.1002/ELAN.200503415.
21. Des Azevedo, S.; Lakshmi, D.; Chianella, I.; Whitcombe, M.J.; Karim, K.; Ivanova-Mitseva, P.K.; Subrahmanyam, S.; Piletsky, S.A. Molecularly Imprinted Polymer-Hybrid Electrochemical Sensor for the Detection of β -Estradiol. *Ind. Eng. Chem. Res.* **2013**, *52*, 13917–13923, doi:10.1021/IE302999J.
22. Yuan, L.; Zhang, J.; Zhou, P.; Chen, J.; Wang, R.; Wen, T.; Li, Y.; Zhou, X.; Jiang, H. Electrochemical Sensor Based on Molecularly Imprinted Membranes at Platinum Nanoparticles-Modified Electrode for Determination of 17 β -Estradiol. *Biosens. Bioelectron.* **2011**, *29*, 29–33, doi:10.1016/J.BIOS.2011.07.058.
23. Wen, T.; Xue, C.; Li, Y.; Wang, Y.; Wang, R.; Hong, J.; Zhou, X.; Jiang, H. Reduced Graphene Oxide-Platinum Nanoparticles Composites Based Imprinting Sensor for Sensitively Electrochemical Analysis of 17 β -Estradiol. *J. Electroanal. Chem.* **2012**, *682*, 121–127, doi:10.1016/J.JELECHEM.2012.07.015.
24. Magar, H.S.; Hassan, R.Y.A.; Mulchandani, A. Electrochemical Impedance Spectroscopy (EIS): Principles, Construction, and Biosensing Applications. *Sensors* **2021**, *21*, 6578, doi:10.3390/S21196578.
25. Cesiulis, H.; Tsyntaru, N.; Ramanavicius, A.; Ragoisha, G. The Study of Thin Films by Electrochemical Impedance Spectroscopy. *NanoSci. Technol.* **2016**, 3–42, doi:10.1007/978-3-319-30198-3_1.
26. Zhang, X.; Peng, Y.; Bai, J.; Ning, B.; Sun, S.; Hong, X.; Liu, Y.; Liu, Y.; Gao, Z. A Novel Electrochemical Sensor Based on Electropolymerized Molecularly Imprinted Polymer and Gold Nanomaterials Amplification for Estradiol Detection. *Sens. Actuators B Chem.* **2014**, *200*, 69–75, doi:10.1016/J.SNB.2014.04.028.
27. Florea, A.; Cristea, C.; Vocanson, F.; Săndulescu, R.; Jaffrezic-Renault, N. Electrochemical Sensor for the Detection of Estradiol Based on Electropolymerized Molecularly Imprinted Polythioaniline Film with Signal Amplification Using Gold Nanoparticles. *Electrochem. Commun.* **2015**, *59*, 36–39, doi:10.1016/J.ELECOM.2015.06.021.
28. Neese, F. The ORCA program system. *Wiley Interdiscip. Rev.: Comput. Mol. Sci.* **2012**, *2*, 73–78, doi:10.1002/WCMS.81.
29. Neese, F. Software update: The ORCA program system—Version 5.0. *Wiley Interdiscip. Rev.: Comput. Mol. Sci.* **2022**, *12*, 1606, doi:10.1002/WCMS.1606.
30. Neese, F.; Wennmohs, F.; Becker, U.; Riplinger, C. The ORCA quantum chemistry program package. *J. Chem. Phys.* **2020**, *152*, 224108, doi:10.1063/5.0004608.
31. Helmich-Paris, B.; de Souza, B.; Neese, F.; Izsák, R. An improved chain of sphere for exchange algorithm. *J. Chem. Phys.* **2021**, *155*, 104109, doi:10.1063/5.0058766.
32. Becke, A.D.; Density-functional thermochemistry. III. The role of exact exchange. *J. Chem. Phys.* **1993**, *98*, 5648–5652, doi:10.1063/1.464913.
33. Nicholls, I.A.; Andersson, H.S.; Charlton, C.; Henschel, H.; Karlsson, B.C.G.; Karlsson, J.G.; O'Mahony, J.; Rosengren, A.M.; Rosengren, K.J.; Wikman, S. Theoretical and Computational Strategies for Rational Molecularly Imprinted Polymer Design. *Biosens. Bioelectron.* **2009**, *25*, 543–552, doi:10.1016/J.BIOS.2009.03.038.
34. Cenci, L.; Tatti, R.; Tognato, R.; Ambrosi, E.; Piotto, C.; Bossi, A.M. Synthesis and Characterization of Peptide-Imprinted Nanogels of Controllable Size and Affinity. *Eur. Polym. J.* **2018**, *109*, 453–459, doi:10.1016/J.EURPOLYMJ.2018.08.031.
35. Beygisangchin, M.; Rashid, S.A.; Shafie, S.; Sadrollhosseini, A.R.; Lim, H.N. Preparations, Properties, and Applications of Polyaniline and Polyaniline Thin Films—A Review. *Polymers* **2021**, *13*, 2003, doi:10.3390/POLYM13122003.
36. Gvozdenović, M.M.; Jugović, B.Z.; Stevanović, J.S.; Trišović, T.Lj.; Grgur, B.N. Electrochemical Polymerization of Aniline. *Electropolymerization* **2011**, doi:10.5772/28293.
37. Curteanu, S.; Dumitrescu, A.; Mihăilescu, C.; Simionescu, B. Neural Network Modeling Applied to Polyacrylamide Based Hydrogels Synthesized By Single Step Process. *Polym. Plast. Technol. Eng.* **2008**, *47*, 1061–1071, doi:10.1080/03602550802355750.
38. Choudhary, S.; Altintas, Z. Development of a Point-of-Care SPR Sensor for the Diagnosis of Acute Myocardial Infarction. *Biosensors* **2023**, *13*, 229, doi:10.3390/BIOS13020229.
39. Jyoti; Gonzato, C.; Żołek, T.; Maciejewska, D.; Kutner, A.; Merlier, F.; Haupt, K.; Sharma, P.S.; Noworyta, K.R.; Kutner, W. Molecularly Imprinted Polymer Nanoparticles-Based Electrochemical Chemosensors for Selective Determination of Cilostazol and Its Pharmacologically Active Primary Metabolite in Human Plasma. *Biosens. Bioelectron.* **2021**, *193*, 113542, doi:10.1016/J.BIOS.2021.113542.

1
2 SYNOPSIS TOC
3 TOC/Abstract Graphic:
4
5



1
2
3
4
5
6
7
8
9
10
11
12
13
14
15
16
17
18
19
20
21
22
23
24
25
26
27
28
29
30
31
32
33
34
35
36
37
38
39
40
41
42
43
44
45
46
47
48
49
50
51
52
53
54
55
56
57
58
59
60

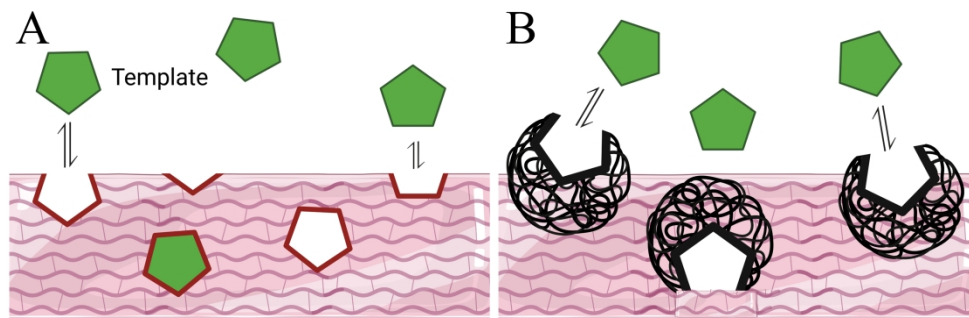


Figure 1. Scheme depicting the heterogeneity of binding sites formed by means of the molecularly imprinting process, in the case of electropolymerization of PANI (A); homogeneous binding sites obtained by doping with nanoMIPs PANI (B).

370x120mm (300 x 300 DPI)

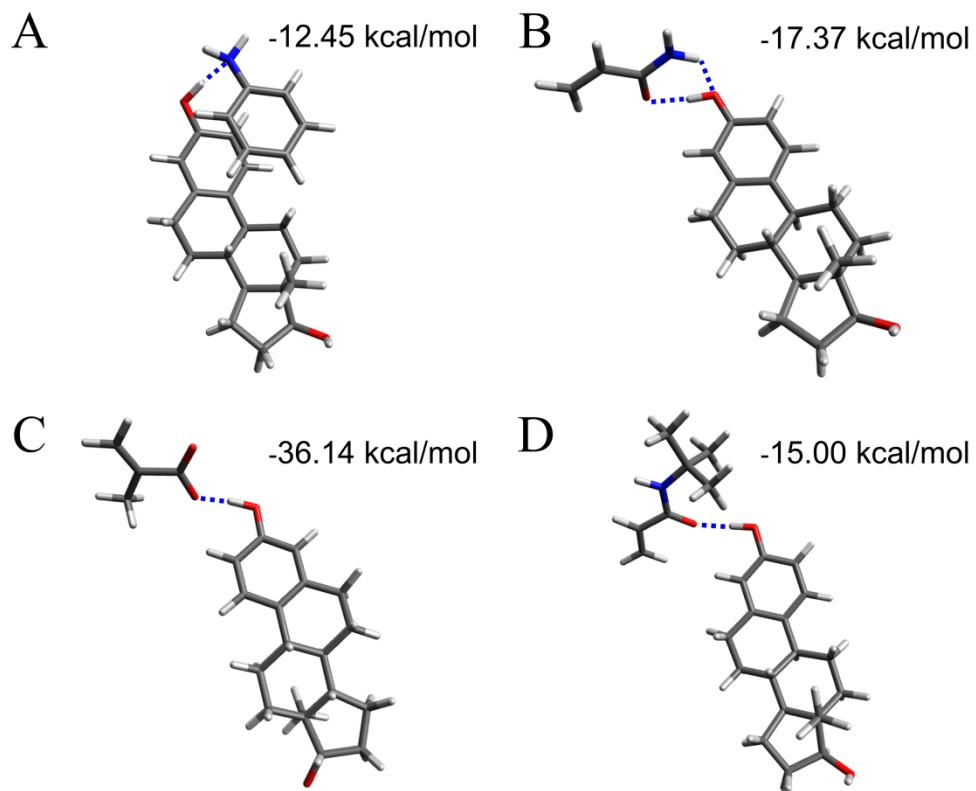


Figure 2. Molecular modelling. Sketches of the interaction between E2 and the monomers: Aniline (A), Acrylamide (B), Methacrylic acid (C) and tert-butylacrylamide (D).

339x273mm (300 x 300 DPI)

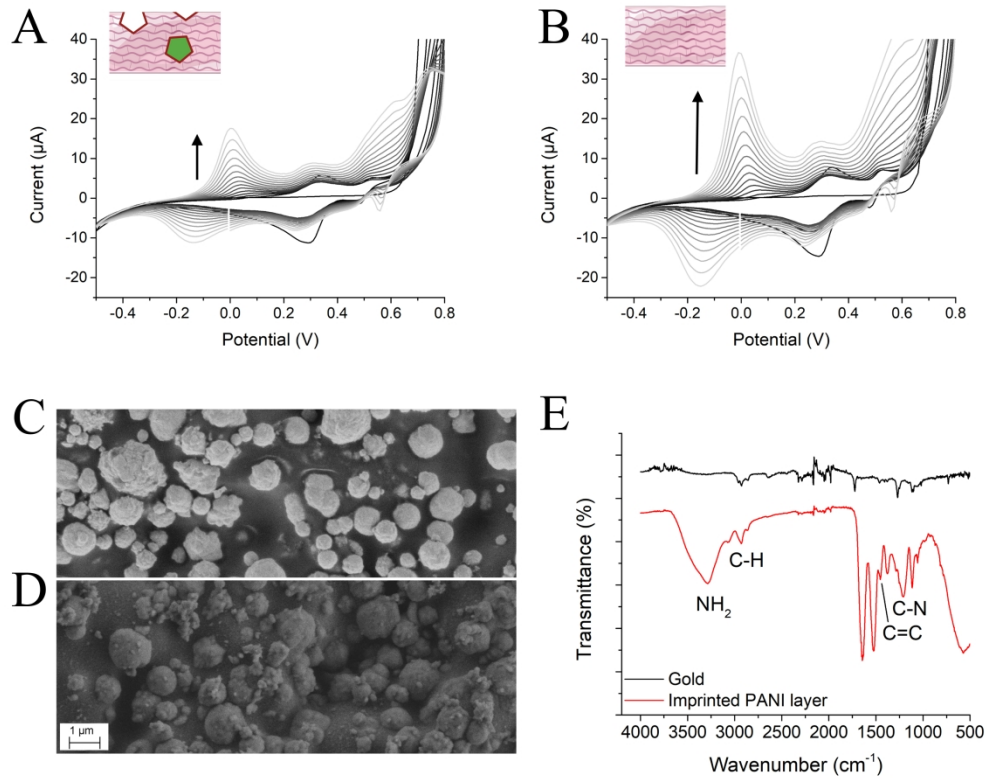


Figure 3. CV of Imprinted PANI layer (A) and of PANI control (B). SEM image of bare electrode (C) and Imprinted PANI layer (D) FT-IR spectra (E).

347x275mm (300 x 300 DPI)

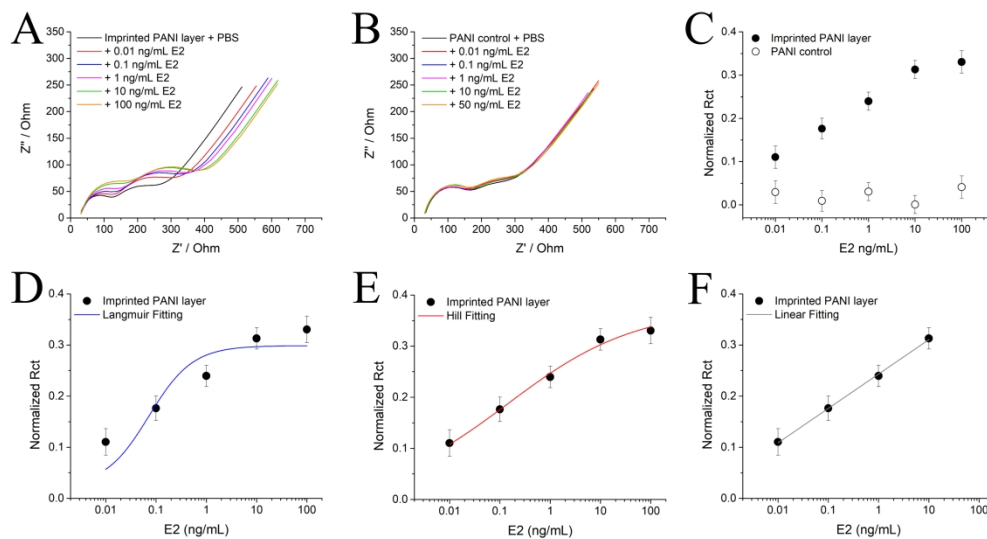


Figure 4. Nyquist plot of Imprinted PANI layer (A) and of PANI control (B) incubated with increasing concentrations of E2. Normalized Rct as function of E2 concentrations of Imprinted PANI layer and PANI control (C). Imprinted PANI layer fitted with Langmuir (D), Hill (E) and Linear (F) equation models.

379x205mm (300 x 300 DPI)

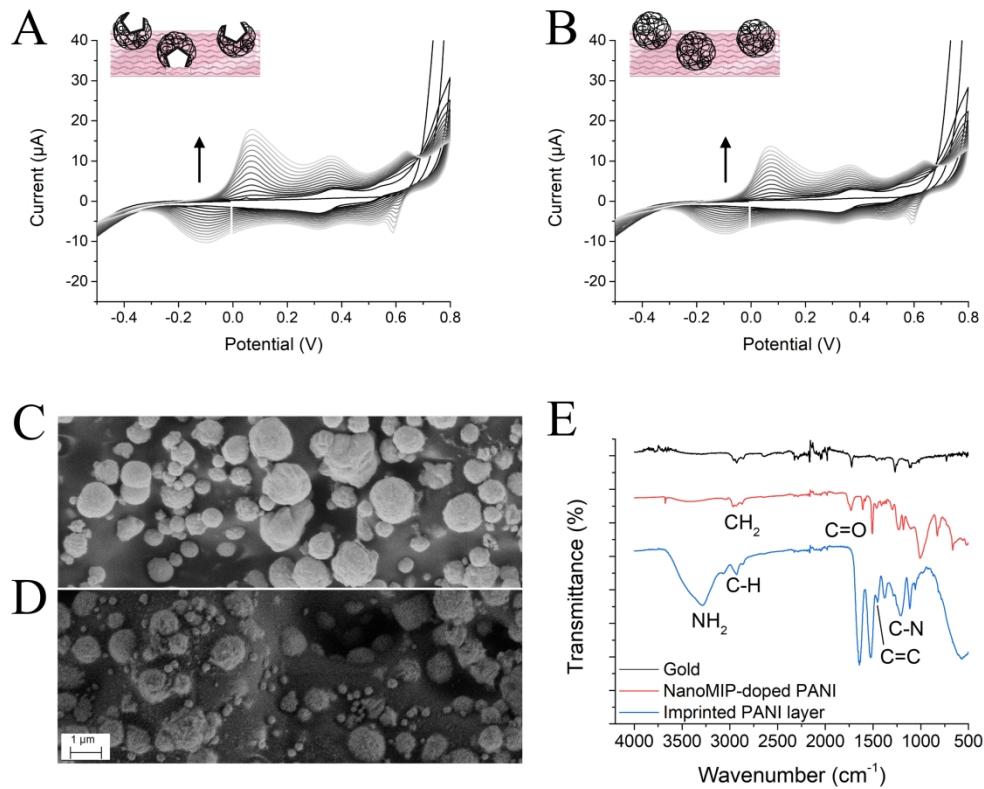


Figure 5. CV of nanoMIP-doped PANI (A) and of control NPs-doped PANI (B). SEM image of bare electrode (C) and of nanoMIP-doped PANI (D). FT-IR spectra (E).

343x273mm (300 x 300 DPI)

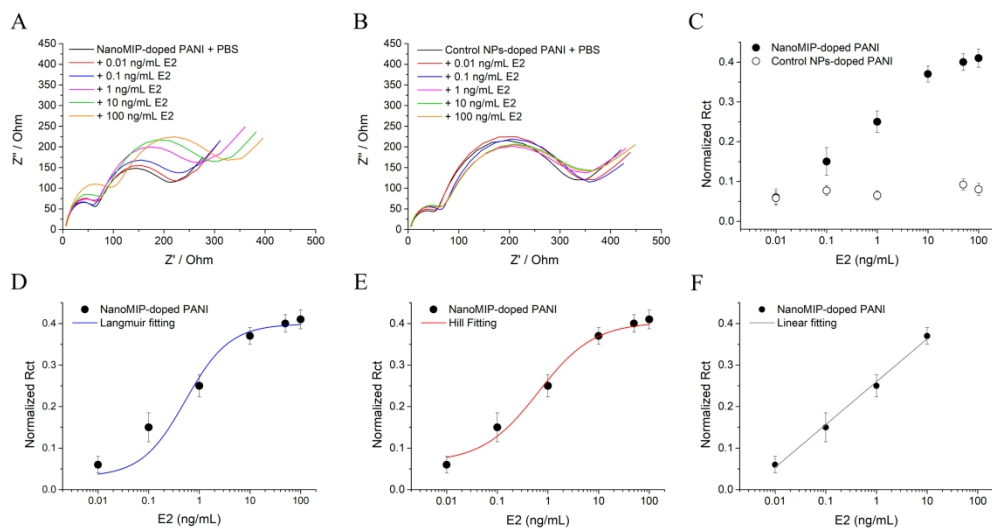
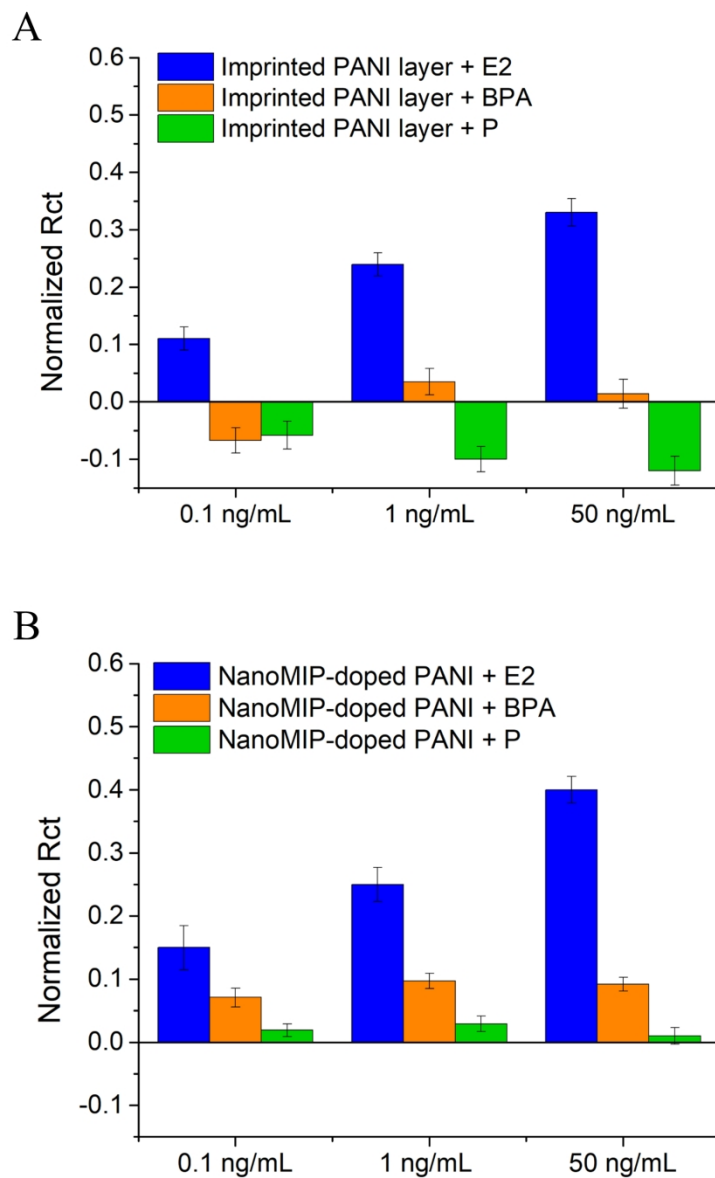


Figure 6. Nyquist plot of nanoMIP-doped PANI (A) and of control NP-doped PANI (B) incubated with increasing concentrations of E2. Normalized Rct as a function of E2 concentration of nanoMIP-doped PANI and control NP-doped PANI (C). NanoMIP-doped PANI fitted with Langmuir (D), Hill (E) and Linear (F) equation model.

376x200mm (300 x 300 DPI)



45 Figure 7. Normalized Rct of Imprinted PANI layer (A) and nanoMIP-doped PANI (B) incubated with E2 (blue
46 bar), BPA (orange bar) and P (green bar) at different concentrations.

47 155x250mm (300 x 300 DPI)

48
49
50
51
52
53
54
55
56
57
58
59
60

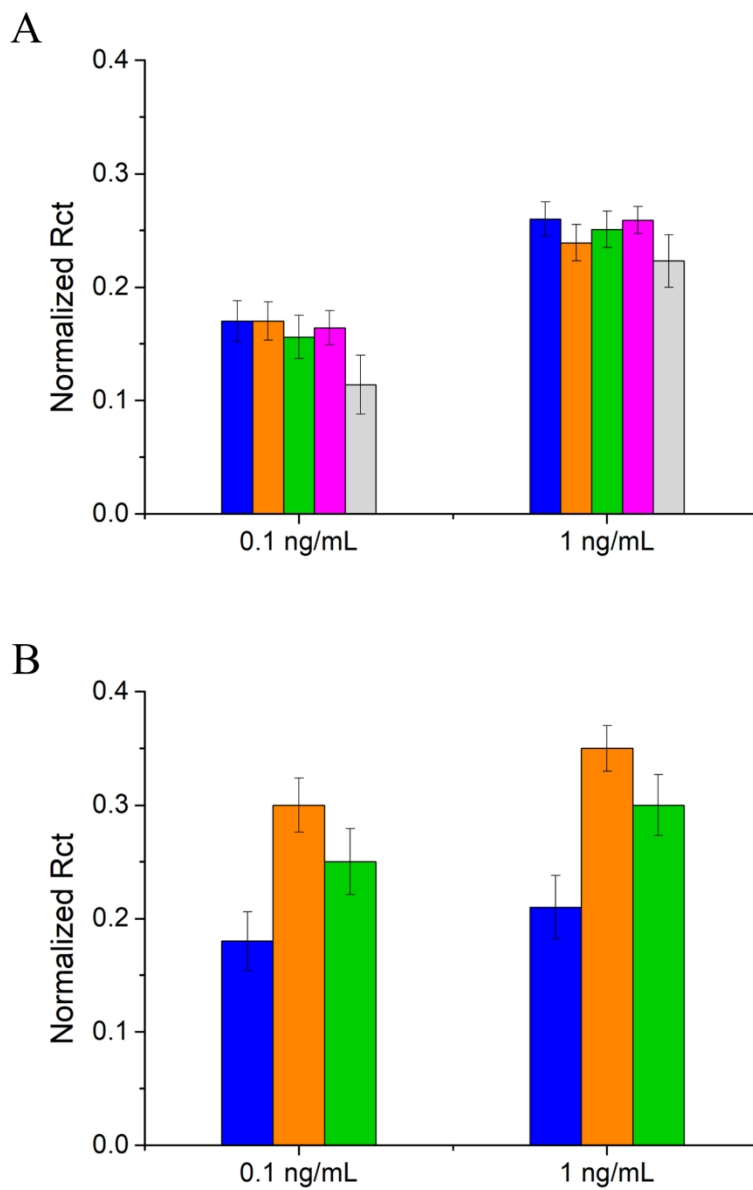


Figure 8. Reproducibility of nanoMIPs-doped PANI (A) and of Imprinted PANI layer (B).

155x235mm (300 x 300 DPI)

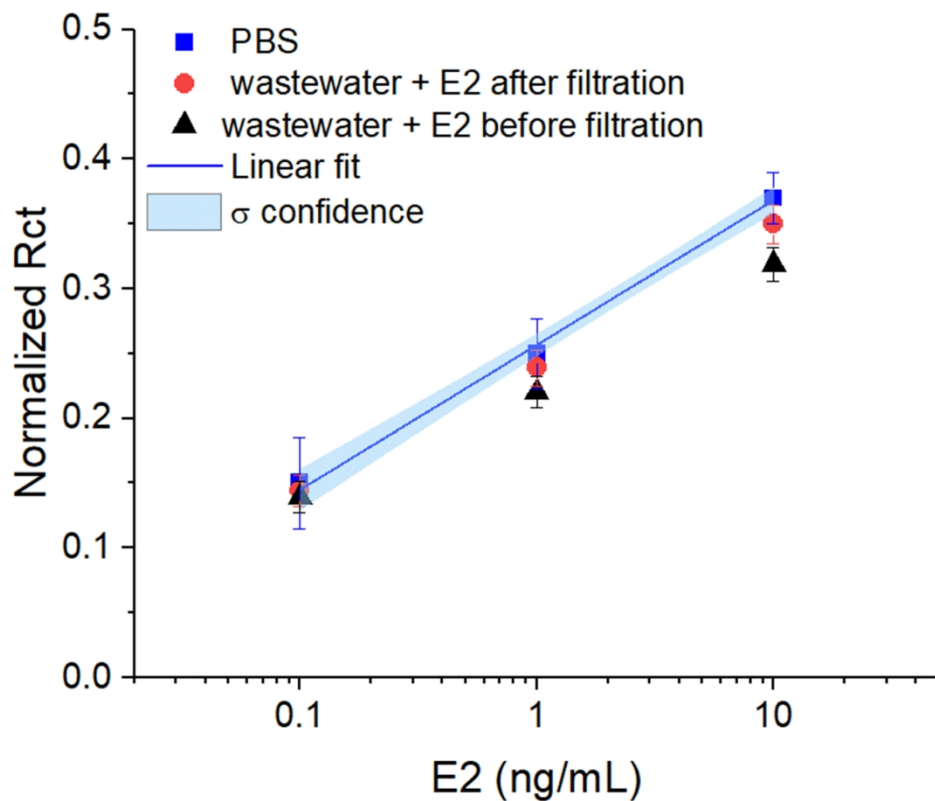
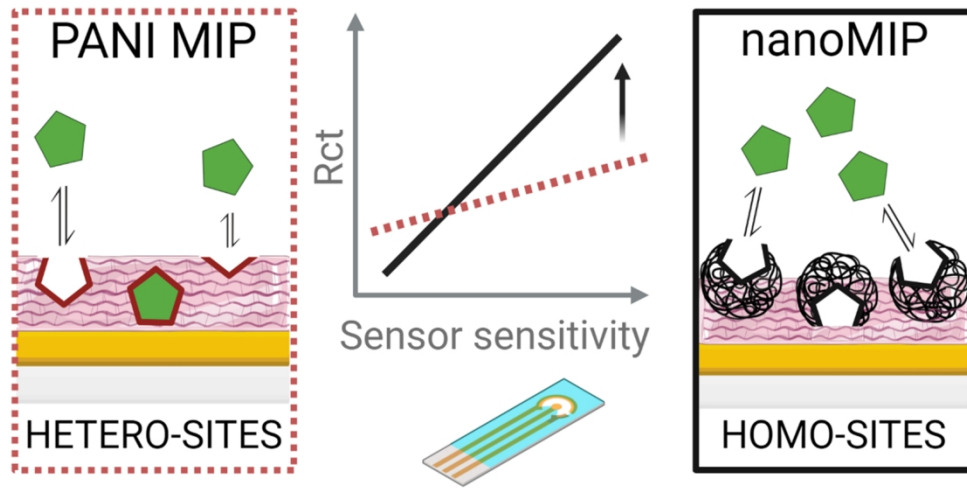


Figure 9. Normalized Rct as a function of E2 concentration of the EIS-nanoMIP-doped PANI sensor incubated with wastewater spiked with different concentrations of E2 before filtration (black triangles), or after filtration (red dots) compared to the E2 measurements in PBS (blue squares); linear fit of E2 in PBS $y=0.111x + 0.256$ (blue line); light blue halo represents the 1 σ confidence level for the fitting.

172x145mm (300 x 300 DPI)

1
2
3
4
5
6
7
8
9
10
11
12
13
14
15
16
17
18
19
20
21
22
23
24
25
26
27
28
29
30
31
32
33
34
35
36
37
38
39
40
41
42
43
44
45
46
47
48
49
50
51
52
53
54
55
56
57
58
59
60



Graphical abstract TOC

146x81mm (300 x 300 DPI)